DEUTSCHES ELEKTRONEN-SYNCHROTRON
Ein Forschungszentrum der Helmholtz-Gemeinschaft

DESY 20-113
arXiv:2007.03696
July 2020

Precise Dark Matter Relic Abundance in Decoupled Sectors

T. Bringmann

Department of Physics, University of Oslo, Norway

P. F. Depta, M. Hufnagel, K. Schmidt-Hoberg

Deutsches Elektronen-Synchrotron DESY, Hamburg

ISSN 0418-9833

NOTKESTRASSE 85 - 22607 HAMBURG

DESY Zentralbibliothek Notkestraße 85 22607 Hamburg Germany	DESY Bibliothek Platanenallee 6 15738 Zeuthen Germany

DESY 20-113

Precise dark matter relic abundance in decoupled sectors

Torsten Bringmann*
Department of Physics, University of Oslo, Box 1048, N-0316 Oslo, Norway

Paul Frederik Depta,† Marco Hufnagel,‡ and Kai Schmidt-Hoberg§
Deutsches Elektronen-Synchrotron DESY, Notkestraße 85, D-22607 Hamburg, Germany

Dark matter (DM) as a thermal relic of the primordial plasma is increasingly pressured by direct and indirect searches, while the same production mechanism in a decoupled sector is much less constrained. We extend the standard treatment of the freeze-out process to such scenarios and perform precision calculations of the annihilation cross section required to match the observed DM abundance. We demonstrate that the difference to the canonical value is generally sizeable, and can reach orders of magnitude. Our results directly impact the interpretation of DM searches in hidden sector scenarios.

arXiv:2007.03696v1 [hep-ph] 7 Jul 2020

Introduction.— Cosmological observations require the existence of a dark matter (DM) component making up about 80 % of the matter in our Universe [1], likely consisting of a new type of elementary particle [2, 3]. The most often adopted paradigm for the production of such particles is via freeze-out from the primordial plasma of standard model (SM) particles [4]. This roughly requires weak-scale couplings for DM masses at the electroweak scale – which has been argued to be an intriguing coincidence in view of proposed solutions to the hierarchy problem of the SM [5] – but the same mechanism also works for lighter DM and correspondingly weaker couplings [6]. The formalism to calculate the thermal relic abundance in these scenarios [7, 8] is well established and successfully used in a plethora of applications, *e.g.* for benchmarking the reach of experimental searches for non-gravitational DM interactions [1, 9–13]. Based on this standard prescription, several public numerical codes [14–17] provide precision calculations of the DM abundance, matching the percent level observational accuracy.

More recently, the focus has shifted to models where DM couples much more strongly to particles in a 'secluded' dark sector than to any of the SM particles [18–22]. This development is partially motivated by the fact that more traditional DM candidates are increasingly pressured by the absence of undisputed signals in direct searches as well as at colliders [23–25], but also from a theoretical perspective there is no fundamental argument why DM – or other new elementary particles – should be charged under the SM gauge group. Remarkably, thermal freeze-out works equally well also in these models, providing a compelling potential explanation for the observed DM abundance. As a consequence, couplings needed to achieve this goal are often either implicitly fixed or explicitly targeted in various searches for hidden sector particles [26–33].

Despite this development, relic density calculations in dark sector models have not yet reached the same level of precision as for freeze-out scenarios in the visible sector, although a number of interesting effects which possibly impact the dark matter abundance have been identified [19, 34–36]. In this work we update previous treatments by self-consistently taking into account all relevant effects, including some that have so far been neglected. We present highly accurate results for the annihilation cross section required to obtain the correct relic density in these scenarios, matching for the first time the precision of corresponding predictions in the standard case [37].

Standard freeze-out.— We start by briefly revisiting the canonical approach. The number density n_i of dark matter particles $i = \chi, \bar{\chi}$ initially in thermal equilibrium with the SM heat bath at temperature T is described by the Boltzmann equation [7]

$$\frac{\mathrm{d}n_i}{\mathrm{d}t} + 3Hn_i = \langle\sigma v\rangle \left(n_{\chi,\mathrm{eq}} n_{\bar{\chi},\mathrm{eq}} - n_\chi n_{\bar{\chi}}\right) , \qquad (1)$$

where H is the Hubble rate,

$$\langle\sigma v\rangle = \int_1^\infty \mathrm{d}\tilde{s}\, \sigma v_{\mathrm{lab}} \frac{2x\sqrt{\tilde{s}-1}(2\tilde{s}-1)K_1\left(2\sqrt{\tilde{s}}x\right)}{{K_2}^2(x)} , \qquad (2)$$

and $n_{\chi,\mathrm{eq}} = n_{\bar{\chi},\mathrm{eq}} = g_\chi m_\chi^3 K_2(x)/(2\pi^2 x)$. Here we defined $x \equiv m_\chi/T$, K_j are the modified Bessel functions of order j, g_χ denotes the internal degrees of freedom (d.o.f.) of χ, σ is the total cross-section for DM annihilations, for a center-of-mass energy $\sqrt{s} \equiv 2m_\chi\sqrt{\tilde{s}}$, and v_{lab} is the velocity of one of the DM particles in the rest-frame of the other.

Let us stress two main assumptions that enter in this widely used form of the Boltzmann equation. The first is that the DM particles have a phase-space distribution $f_i \propto f_{\chi,\mathrm{eq}}$, with the equilibrium distribution being well approximated by $f_{\chi,\mathrm{eq}} = \exp(-E_\chi/T)$ for $m_\chi \gg T$, i.e. that kinetic decoupling [38] happens much later than chemical decoupling and freeze-out (see Ref. [39] for a treatment of early kinetic decoupling). The second assumption is that the annihilation products indeed constitute a *heat bath*, in the sense that none of them builds

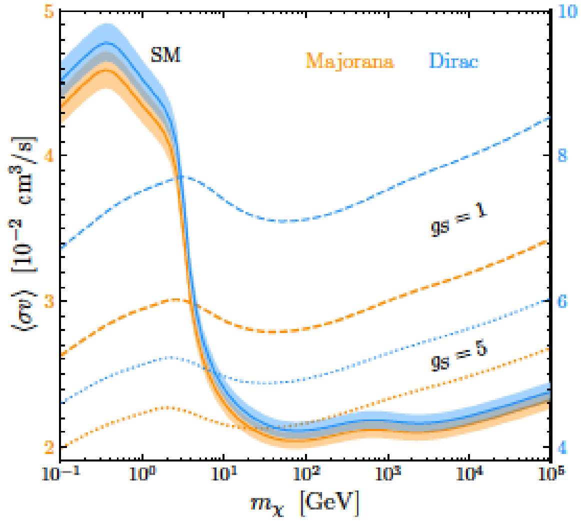

FIG. 1. The value of a constant thermally averaged annihilation rate, $\langle\sigma v\rangle$, resulting in a relic density of Majorana (orange) or Dirac (blue) DM particles matching the observed cosmological DM abundance. Solid lines show the case of DM in equilibrium with the SM until freeze-out (shaded areas indicate the effect of varying $\Omega_{\rm DM}h^2$ within 3σ [1]). Dashed (dotted lines) show the case of DM in equilibrium with a hidden sector containing $g_S = 1$ ($g_S = 5$) light scalar degrees of freedom (with $\mu_S = 0$), which decoupled from the standard model at $T \gg \max[m_\chi, m_t]$. See Appendix A for corresponding results for p-wave annihilation.

up significant chemical potentials. As we will see shortly, both assumptions can be violated in decoupled sectors.

Before doing so, let us first solve Eq. (1) in the standard scenario. In Fig. 1 we indicate with solid lines the value of $\langle\sigma v\rangle$ (assuming a constant value of this quantity around chemical decoupling) that is needed to obtain a relic density matching the observed cosmological DM abundance of $\Omega_{\rm DM}h^2 = 0.120$ [1]. The orange solid lines show the case of Majorana DM (with $g_\chi = 2$ and $\Omega_\chi = \Omega_{\bar\chi} = \Omega_{\rm DM}$), updating the conventionally quoted 'thermal relic cross section' in Ref. [37] with a more recent measurement of $\Omega_{\rm DM}$ and recent lattice QCD results for the evolution of d.o.f. in the early universe [40] (as implemented in DarkSUSY [14]). For comparison, the blue lines indicate the slightly less standard case of Dirac DM (with $g_\chi = g_{\bar\chi} = 2$ and $\Omega_\chi = \Omega_{\bar\chi} = \Omega_{\rm DM}/2$) to stress the not typically appreciated fact that the required value of $\langle\sigma v\rangle$ is *not* exactly twice as large as in the Majorana case.

A secluded dark sector.— The idea [18–22, 26] that DM could be interacting only relatively weakly with the SM, but much more strongly with itself or other particles in a secluded dark sector (DS), has received significant attention [29, 35, 41–46]. In such scenarios, both sectors may well have been in thermal contact at high temperature, until they decoupled at a temperature $T_{\rm dec}$. This results in a non-trivial evolution of the temperature ratio $\xi \equiv T_\chi/T$. As long as the DM interactions with at least one *massless* DS species S are efficient enough to establish thermal equilibrium, entropy is conserved separately in the two sectors and the DS temperature evolves with the effective number of relativistic entropy d.o.f., $g_*^{\rm SM,DS}$, as

$$\xi(T) \equiv \frac{T_\chi(T)}{T} = \frac{\left[g_*^{\rm SM}(T)/g_*^{\rm SM}(T_{\rm dec})\right]^{\frac{1}{3}}}{\left[g_*^{\rm DS}(T)/g_*^{\rm DS}(T_{\rm dec})\right]^{\frac{1}{3}}}\,. \qquad (3)$$

For a precise description of the freeze-out process of χ in such a secluded DS the standard Boltzmann equation (1) then needs to be adapted at three places: both *i)* the equilibrium density $n_{\rm eq}$ and *ii)* the thermal average $\langle\sigma v\rangle$ must be evaluated at T_χ rather than the SM temperature T, and *iii)* the Hubble rate must be increased to take into account the additional energy content residing in the DS. During radiation domination, in particular, this means that $H^2 = (8\pi^3/90)g_{\rm eff}M_{\rm Pl}^{-2}T^4$, where $g_{\rm eff} \simeq g_{\rm SM} + (\sum_b g_b + \frac{7}{8}\sum_f g_f)\xi^4$ and the sum runs over the internal d.o.f. of all fully relativistic DS bosons (b) and fermions (f) (in our numerical treatment, we always use the *full* expression for $g_{\rm eff}$). To the best of our knowledge, precision calculations of the relic density in a decoupled DS that fully and self-consistently implement all three effects have not been performed previously. Here we adapt the relic density routines of DarkSUSY to allow calculations of this kind for a large range of DS models.

Model setup.— Let us for concreteness consider a setup where the DS consists of massive fermions χ, acting as DM, and massless scalars S with $\mu_S = 0$, constituting the heat bath. We assume that the DS decoupled from the SM at high temperatures, such that $g_*^{\rm SM}(T_{\rm dec}) = 106.75$ and $g_*^{\rm DS}(T_{\rm dec}) = g_S + (7/4)N_\chi$ in Eq. (3), where $N_\chi = 1$ ($N_\chi = 2$) for Majorana (Dirac) DM. In Fig. 1 we show the 'thermal' annihilation cross section for $\chi\bar\chi \to SS$ in such a scenario, for different values of g_S. The fact that this differs significantly from the standard case, in comparison to the observational uncertainty in the cosmological DM abundance also indicated in the figure, constitutes our first main result. It is worth stressing that this updated relic density calculation directly applies to a large number of DS models where annihilation proceeds via an s-wave [20, 26, 29, 41, 47–50] (see Appendix A for corresponding results in the case of p-wave annihilation).

To understand the behaviour of the curves shown in Fig. 1, let us first recall that we consider here a constant $\langle\sigma v\rangle$ – which by definition is not affected by a change in ξ. For $g_S = 1$, furthermore, the change in $g_{\rm eff}$ and hence the Hubble rate has only a subdominant effect (but becomes somewhat more important for $g_S = 5$). The main effect visible in the figure thus originates from changing $n_{\chi,\rm eq}(x) \to n_{\chi,\rm eq}(x/\xi)$. For large DM masses and hence freeze-out temperatures, in particular, the heating in the DS due to $\chi\bar{\chi} \to SS$, c.f. the nominator of Eq. (3), is more efficient than the heating in the SM, leading to $\xi > 1$ around freeze-out. This leads to a larger DM density, at a given SM temperature T, which has to be compensated for by a *larger* $\langle\sigma v\rangle$ to match the observed relic abundance. Below DM masses of a few GeV, the drop in the SM d.o.f. until freeze-out is more significant than that in the DS (especially during the QCD phase transition), leading to $\xi < 1$ and hence the need for a *smaller* value of $\langle\sigma v\rangle$ compared to the standard case represented by the solid lines. We note that the value of ξ just before the onset of BBN, on the other hand, does not depend on m_χ for the range of DM masses plotted here. Expressing the final energy density of S in terms of an effective number of relativistic neutrino species, this corresponds to $\Delta N_{\text{eff}} = 0.104(0.202)$ for Majorana DM with $g_S = 1(5)$, and $\Delta N_{\text{eff}} = 0.201(0.275)$ for Dirac DM – which is below current CMB bounds on this quantity, $\Delta N_{\text{eff}} < 0.29$ (95% C.L.) [1], but within reach of next-generation CMB experiments [51, 52].

Chemical potentials during freeze-out.— The above treatment still assumes that the annihilation products constitute or are in equilibrium with a heat bath during the entire chemical decoupling process. This is consistent for massless DS particles S, which retain a vanishing chemical potential during freeze-out due to unavoidable number changing interactions such as $\chi\bar{\chi} \to \chi\bar{\chi}S$. For a fully decoupled DS only containing massive degrees of freedom, however, such interactions are less efficient and may already decouple before freeze-out, implying that *all* particles will generally build up chemical potentials (and not only the DM particles, as in the standard scenario). In order to demonstrate how to correctly describe the evolution of the DS in this more general case, we will consider the same setup as before but mostly focus on DS particles χ and S that are close in mass.

As long as all DS particles remain in kinetic equilibrium, in particular, their phase-space densities are given by Fermi-Dirac or Bose-Einstein distributions with DS temperature T_χ and chemical potentials $\mu_\chi = \mu_{\bar{\chi}}$ and μ_S, respectively. To determine the temporal evolution of these three parameters, we consider the Boltzmann equations for the number densities,

$$\dot{n}_\chi + 3Hn_\chi = \mathfrak{C}/N_\chi, \quad \dot{n}_S + 3Hn_S = -\mathfrak{C}\,, \qquad (4)$$

where the integrated collision operator $\mathfrak{C}$ is specified in Appendix B, as well as energy conservation in the DS during freeze-out, $\nabla_\mu T^{0\mu}_{\text{DS}} = 0$. The latter takes the form

$$\dot{\rho}_{\text{DS}} + 3H\left[\rho_{\text{DS}} + P_{\text{DS}}\right] = 0\,, \qquad (5)$$

with total energy density $\rho_{\text{DS}} \equiv N_\chi \rho_\chi + \rho_S$ and pressure $P_{\text{DS}} \equiv N_\chi P_\chi + P_S$. Note that Eqs. (4) and (5) generally do not imply entropy conservation. However, we find that the respective change in entropy is negligible for all practical calculations we consider. The final step is to note that, since χ and S stay in kinetic equilibrium for all relevant temperatures, all cosmological quantities $Q \in \{n_a, \rho_a, P_a \,|\, a \in \{\chi, \bar{\chi}, S\}\}$ can be interpreted as functions of T_χ, μ_χ and μ_S. Consequently, the relation

$$\dot{Q} = \frac{\partial Q}{\partial T_\chi}\dot{T}_\chi + \frac{\partial Q}{\partial \mu_\chi}\dot{\mu}_\chi + \frac{\partial Q}{\partial \mu_S}\dot{\mu}_S \qquad (6)$$

can be used to transform Eqs. (4) and (5) into a set of differential equations for T_χ, μ_χ and μ_S, which we solve numerically (with $\mu_\chi = \mu_{\bar{\chi}} = \mu_S$ as initial condition).

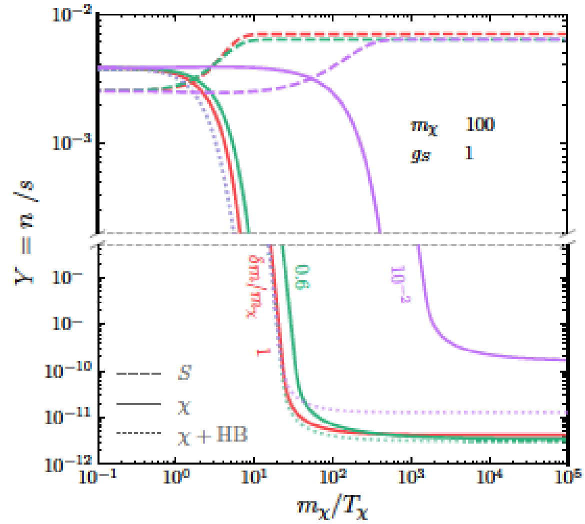

FIG. 2. Evolution of particle abundances Y_a for χ (solid lines) and S (dashed lines), as a function of $x/\xi = m_\chi/T_\chi$, for different mass ratios $\delta m/m_\chi \equiv (m_\chi - m_S)/m_\chi = (1, 0.6, 10^{-2})$. For comparison, dotted lines indicate how the DM abundance Y_χ would evolve when instead using the standard Boltzmann equation (1) assuming thermal equilibrium of S with an additional massless DS heat bath particle. All curves are based on the same $\left|\overline{\mathcal{M}}_{\chi\bar{\chi}\to SS}\right|^2 = const.$, adjusted to give the correct relic density in the limit $m_S \to 0$.

In Fig. 2 we demonstrate the resulting evolution of the particle abundances $Y \equiv n/s$, with s the total entropy density in the SM and DS. For definiteness we choose a Majorana DM particle with $m_\chi = 100\,\text{GeV}$ and a constant annihilation *amplitude* that would result in the correct relic density in the standard treatment (translating to a value of $\langle\sigma v\rangle_{T_\chi \to 0}$ about 10% larger than the orange lines in Fig. 1). The red curves show the case of $m_S = 0$ for which, following the discussion above, we explicitly set $\mu_S = 0$. The resulting evolution of χ (red solid line) therefore coincides exactly with the result of the standard treatment of solving Eq. (1). We note that the increase in Y_S around $T_\chi \sim m_\chi$ is due to the Boltzmann suppression of χ, analogous to the increase in n_γ/s during e^+e^- annihilation in the SM.

For more degenerate masses (green and purple lines in

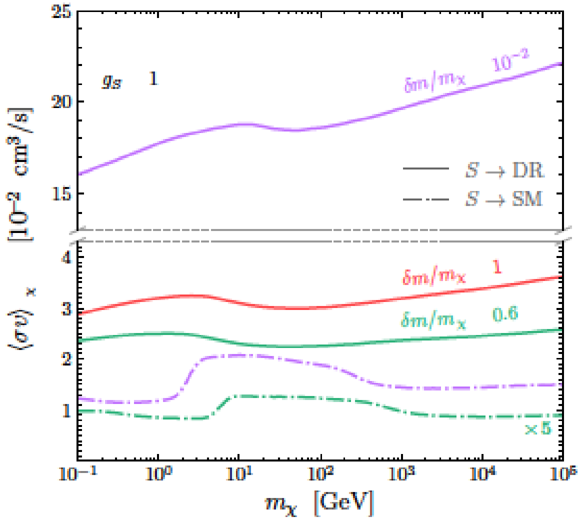

FIG. 3. The required value of the thermally averaged annihilation rate, $\langle \sigma v \rangle_{T_\chi \to 0}$, that results in a relic density of Majorana DM particles with a constant $|\overline{\mathcal{M}}_{\chi\chi \to SS}|^2$ matching the observed DM abundance. Colors correspond to the same mass ratios as in Fig. 2, while the line style distinguishes whether S decays into dark radiation (solid, independent of lifetime τ_S) or into SM states (dash-dotted, for $\tau_S = 1\,\mathrm{s} \times (1\,\mathrm{GeV}/m_S)^2$).

Fig. 2), we allow all chemical potentials to evolve freely. This leads to a rise in μ_S, compensating the would-be Boltzmann suppression of S, and an asymptotic abundance $Y_S^{\mathrm{final}} \approx Y_S^{\mathrm{initial}} + Y_\chi^{\mathrm{initial}}$ because $Y_\chi^{\mathrm{initial}} \gg Y_\chi^{\mathrm{final}}$. The greater number of S particles then delays the Boltzmann suppression of n_χ from around $T_\chi \sim m_\chi$ to when the mean kinetic energy of S drops below δm, roughly around $T_\chi \sim \delta m$. For reference we also show an application of Eq. (1) (dotted lines) assuming thermal equilibrium of S with additional massless DS heat bath particles such that $\mu_S = 0$ and $T_\chi \propto a^{-1}$ with the scale factor a. Comparing the purple lines ($\delta m/m_\chi = 10^{-2}$), *e.g.*, Boltzmann suppression of χ for the solid line occurs at temperatures T_χ around two orders of magnitude smaller than for the dotted line, or a one order of magnitude larger ($T_\chi \propto a^{-2}$ at $T_\chi \lesssim m_S$ for the solid line). Approximating the annihilation rate by $\langle \sigma v \rangle n_\chi^2 \propto a^{-6}$, whereas the dilution by cosmic expansion is $3H n_\chi \propto a^{-5}$, this implies that freeze-out happens when χ is less Boltzmann-suppressed and Y_χ is enhanced by $\sim a$, i.e. around one order of magnitude. In general, the correct treatment of the chemical potentials thus leads to an enhanced DM abundance compared to the 'naïve' assumption of $\mu_S = 0$ and $T_\chi \propto a^{-1}$. Comparing instead to the $m_S = 0$ case, c.f. the standard situation depicted in Fig. 1, Y_χ^{final} first decreases up to a mass ratio of $m_S/m_\chi = 0.4$ (green lines), then increases again with S and χ becoming more and more degenerate.

For S close in mass to χ, the final DM relic abundance will not only depend on the decoupling process but also on how S decays after freeze-out. If S was stable, in particular, it would simply contribute to the total DM density, by far overshooting the observed value (unless allowing for sufficiently small temperature ratios $\xi_{T\to\infty} \ll 1$, thus relaxing our assumption of initial thermal contact between SM and DS). In Fig. 3 we explore two concrete decay scenarios, by showing the 'thermal' annihilation cross section for the same mass ratios as discussed in Fig. 2.[1] The first scenario is S decaying to effectively massless DS states, or dark radiation (DR), and indicated by solid lines. The additional effective relativistic d.o.f. resulting from the decay of S will in general depend on the lifetime τ_S, because the energy densities of matter and radiation red-shift differently. As already for $m_S = 0$ one has $\Delta N_{\mathrm{eff}} = 0.104$ (see above), the case $m_S \sim m_\chi$ is generally in conflict with the CMB limit even if the decay happens shortly after freeze-out. The second example (dash-dotted lines) considers S decays to SM states. In this case, the resulting entropy injection into the SM plasma will lead to a dilution of DM, lowering the required DM annihilation cross section. This effect has recently been argued to allow for DM masses above the naïve unitarity limit [36, 53, 54]. Note that the lifetime $\tau_S = 1\,\mathrm{s} \times (1\,\mathrm{GeV}/m_S)^2$ chosen here for illustration is expected to be in conflict with observations of primordial element abundances for $\tau_S > 0.1\,\mathrm{s}$ [55], i.e. $m_S \lesssim 3\,\mathrm{GeV}$.

To summarize, the solid lines in Fig. 3 show the required DM annihilation cross section to obtain the observed DM abundance assuming S decays *without* injecting entropy in the SM and thus diluting the DM abundance. These therefore provide an *upper* limit to scenarios where S decays into the SM after DM freeze-out, as exemplary illustrated by the dash-dotted lines. It is evident that the required DM annihilation cross section can be very different from the canonical value shown in Fig. 1, in particular for small mass differences. In the extreme case of degenerate masses, $m_S = m_\chi$, no Boltzmann suppression of χ can occur – independently of the DM annihilation cross section – implying that the observed DM abundance can only be achieved for sufficiently small temperature ratios $\xi_{T\to\infty} \ll 1$ as discussed above for a stable S.

Discussion.— For the choice of parameters discussed above we explicitly checked, c.f. Appendix B, that the assumption of kinetic equilibrium is always satisfied during the freeze-out process, justifying our ansatz for the phase-space distributions f_a. Let us stress that this is particu-

[1] This is implemented by adding $-n_S/\tau_S$ to the r.h.s. of Eq. (4) for n_S, $-m_S n_S/\tau_S$ to the r.h.s. of Eq. (5), and an additional energy density in dark radiation $\dot\rho_{\mathrm{DR}} + 4H\rho_{\mathrm{DR}} = m_S n_S/\tau_S$ for decays in effectively massless DS states, or $\dot\rho_{\mathrm{SM}} + 3H(\rho_{\mathrm{SM}} + P_{\mathrm{SM}}) = m_S n_S/\tau_S$ for decays into SM particles.

larly important for small mass splittings, where $\mu_S \simeq m_S$ makes it mandatory to include the full quantum statistics for all particles. The commonly used assumption of a Maxwell-Boltzmann distribution is, in other words, no longer justified and leads to quantitatively wrong results in the relic density calculation.

So far we have focussed on a fully secluded DS, in which case the most prominent observables to test such models are $\Omega_{\rm DM}$ and $\Delta N_{\rm eff}$. It is however worth mentioning that in many models there are additional tiny couplings to the SM that would allow further experimental signatures. A setup where hidden sector freeze-out can naturally occur while still allowing for sufficiently large couplings to the SM to be probed by particle physics experiments, *e.g.*, are scalar or pseudoscalar mediators with Yukawa-like coupling structure [30, 32, 33, 56–58]. Also indirect DM searches for secluded dark sectors [59] provide a potentially promising avenue, in particular for the strongly enhanced annihilation rates necessary to accommodate DM degenerate in mass with its annihilation products.

Conclusions.— In this work we have presented a framework for precision calculations of DM freeze-out in a secluded sector, matching the observational accuracy on the one hand, and the increasing demand for consistent interpretations of phenomenological dark sector studies on the other hand. We have provided new benchmark 'thermal' annihilation cross sections for relativistic heat bath particles, and demonstrated that the difference to the standard treatment can be even larger for non-relativistic DM annihilation products. The latter case is intrinsically strongly model-dependent, and will be studied in more detail elsewhere. Further interesting extensions, not the least in view of the significant model-building activity in these areas, would be to generalise the precision relic calculations presented here to models where the DM particles in the hidden sector do not obey a Z_2 symmetry [60–62], are asymmetric [63] or have a relic abundance set by freeze-in rather than freeze-out [64, 65].

Acknowledgements.— This work is supported by the ERC Starting Grant 'NewAve' (638528) as well as by the Deutsche Forschungsgemeinschaft under Germany's Excellence Strategy – EXC 2121 'Quantum Universe' – 390833306.

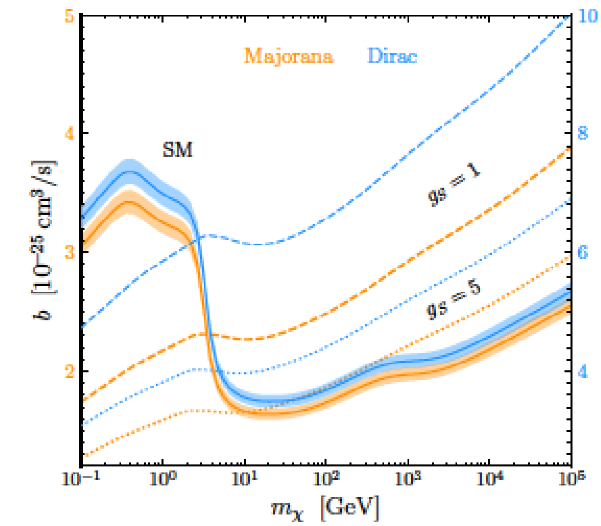

FIG. 4. Same as Fig. 1 in the main text, but for p-wave annihilation with $\sigma v_{\rm lab} = b\, v_{\rm lab}^2$.

A. DM annihilation via p-wave

In the case of s-wave annihilation to massless final states, the velocity-weighted annihilation cross section is constant in the limit of small DM velocities, resulting in $\langle\sigma v\rangle = \sigma v_{\rm lab}$. This simplified ansatz for $\langle\sigma v\rangle$ (neglecting higher-order contributions in v, following common practice) has been presented in Fig. 1 in the main text, both for DM annihilating to SM particles and for situations in which the relic abundance is set via freeze-out in a hidden sector.

Here we complement this by considering instead the case of p-wave annihilation, which also has been frequently considered for DS freeze-out production of DM [29, 30, 32, 49, 56–58]. To describe such models, we will again take a simplified ansatz for the cross section by only keeping the leading term in the DM velocities,

$$\sigma v_{\rm lab} = b\, v_{\rm lab}^2\,, \tag{7}$$

where we assume b to be constant. For the thermally averaged cross section entering in the Boltzmann equation, Eq. (1), this implies $\langle\sigma v\rangle = b \times \left[6(x/\xi)^{-1} - 27(x/\xi)^{-2} + ...\right]$. The value of b resulting in the correct DM relic abundance in this case is shown in Fig. 4, for the same choice of DM models (Dirac and Majorana fermions, respectively) and heat bath components as in Fig. 1 in the main text.

In comparison, the main differences in these figures are that *i)* the value of b resulting in the correct relic density is about one order of magnitude larger than the value of $\langle\sigma v\rangle$ required in the case of s-wave annihilation and that *ii)* this 'thermal' value of b rises faster with m_χ than its s-wave counterpart. Both of this can be traced back to the fact that also for p-wave annihilation it is $\langle\sigma v\rangle$ around chemical decoupling, and not b, that sets the relic density. In the SM case, e.g., $b/\langle\sigma v\rangle \approx x_{\rm cd}/6$, where $x_{\rm cd}$ depends logarithmically on the DM mass and rises from $x_{\rm cd} \approx 18.8$ (for $m_\chi = 100\,{\rm MeV}$) to $x_{\rm cd} \approx 31.6$ (for $m_\chi = 100\,{\rm TeV}$). The above estimate should be corrected by another factor of about 2 because decoupling does not happen instantaneously, and $\int {\rm d}T\langle\sigma v\rangle^{p-{\rm wave}}/\int {\rm d}T\langle\sigma v\rangle^{s-{\rm wave}} \approx 1/2$ (as first stressed in Ref. [66]). The same general trend, finally, is also visible for annihilations in the hidden sector, with $\xi \neq 1$. Compared to Fig. 1, furthermore, the difference between SM and DS results is somewhat larger because ξ enters directly in $\langle\sigma v\rangle$.

B. Collision term including chemical potential

For general two-body annihilation processes $\chi\bar\chi \leftrightarrow SS'$, and assuming CP-invariance, the integrated collision operator from Eq. (4) in the main text takes the form

$$\mathfrak{C} = 2g_\chi^2 \int (2\pi)^4 \delta(p_\chi + p_{\bar\chi} - p_S - p_{S'}) |\overline{\mathcal{M}}_{\chi\bar\chi\to SS'}|^2 \times \left[f_S f_{S'}(1-f_\chi)(1-f_{\bar\chi}) - f_\chi f_{\bar\chi}(1+f_S)(1+f_{S'})\right] \times {\rm d}\Pi_\chi {\rm d}\Pi_{\bar\chi} {\rm d}\Pi_S {\rm d}\Pi_{S'}\,, \tag{8}$$

where ${\rm d}\Pi_a = {\rm d}^3 p_a/(2\pi)^3 2E_a$ and $|\overline{\mathcal{M}}_{\chi\bar\chi\to SS'}|^2$ is the squared matrix element, averaged (summed) over the spins of all initial (final) state particles. We assume all involved particles to be in kinetic equilibrium, i.e. the phase-space distributions take the form $f_a = 1/[e^{(E_a-\mu_a)/T_\chi} \pm 1]$, with $a \in \{\chi, \bar\chi, S, S'\}$ and the $-$ $(+)$ sign is used for bosons (fermions). In the special case of a constant matrix element – which is justified for contact-like interactions and which we adopt as benchmark scenario in the main text – Eq. (8) can be simplified to

$$\mathfrak{C} = \frac{g_\chi^2 |\overline{\mathcal{M}}_{\chi\bar\chi\to SS}|^2}{512\pi^5 N_\chi^{-1}} \int_{m_\chi}^\infty \int_{m_\chi}^\infty \int_{-1}^1 p_\chi p_{\bar\chi} \mathcal{K}\, {\rm d}\cos\theta {\rm d}E_\chi {\rm d}E_{\bar\chi}\,, \tag{9}$$

Moreover,

$$\mathcal{K} \equiv \alpha_*(1-f_\chi)(1-f_{\bar\chi}) - f_\chi f_{\bar\chi}\left(\beta + 2\alpha + \alpha_*\right)\,, \tag{10}$$

with

$$\beta \equiv \sqrt{1 - \frac{4m_S^2}{E'^2 - p'^2}}\,, \tag{11}$$

$$\alpha \equiv \frac{T_\chi}{p'} \log\left[\frac{e^{E'/T_\chi} - e^{(E'-p'\beta+2\mu_S)/(2T_\chi)}}{e^{E'/T_\chi} - e^{(E'+p'\beta+2\mu_S)/(2T_\chi)}}\right]\,, \tag{12}$$

$$\alpha_* \equiv \frac{\beta + 2\alpha}{e^{(E'-2\mu_S)/T_\chi} - 1}\,, \tag{13}$$

where $p' \equiv |\vec p_\chi + \vec p_{\bar\chi}| = (p_\chi^2 + p_{\bar\chi}^2 + 2p_\chi p_{\bar\chi}\cos\theta)^{1/2}$ and $E' \equiv E_\chi + E_{\bar\chi}$.

For highly non-relativistic DM, the annihilation cross section for a constant matrix element becomes independent of the center-of-mass energy, and hence $\sigma v_{\rm lab} \simeq \langle\sigma v\rangle$. In this limit, annihilation cross section and amplitude are related as

$$|\overline{\mathcal{M}}_{\chi\bar\chi\to SS}|^2 \simeq \frac{16\pi m_\chi^2}{\sqrt{1 - m_S^2/m_\chi^2}} \langle\sigma_{\chi\bar\chi\to SS} v\rangle_{T_\chi\to 0}\,. \tag{14}$$

In the simplest models, the same constant matrix element also describes the scattering process $\chi S \leftrightarrow \chi S$, in which case the above expression provides a convenient means of estimating the time of kinetic decoupling for a given value of $\langle\sigma v\rangle$. For $m_\chi \sim m_S$, e.g., this happens when the scattering rate falls behind the Hubble rate, $n_S\langle\sigma_{\chi S\leftrightarrow\chi S} v\rangle \sim H$, while for $m_\chi \gg m_S$ it is instead the (smaller) momentum exchange rate γ that provides the relevant scale (see, e.g., Refs. [38, 39]). Using this condition, we explicitly checked that S and χ remain in kinetic equilibrium during the freeze-out process.

* torsten.bringmann@fys.uio.no
† frederik.depta@desy.de
‡ marco.hufnagel@desy.de
§ kai.schmidt-hoberg@desy.de

[1] N. Aghanim *et al.* (Planck), Planck 2018 results. VI. Cosmological parameters, (2018), arXiv:1807.06209 [astro-ph.CO].

[2] G. Jungman, M. Kamionkowski, and K. Griest, Supersymmetric dark matter, Phys. Rept. **267**, 195 (1996), arXiv:hep-ph/9506380.

[3] G. Bertone, D. Hooper, and J. Silk, Particle dark matter: Evidence, candidates and constraints, Phys. Rept. **405**, 279 (2005), arXiv:hep-ph/0404175.

[4] B. W. Lee and S. Weinberg, Cosmological Lower Bound on Heavy Neutrino Masses, Phys. Rev. Lett. **39**, 165 (1977).

[5] J. R. Ellis, J. Hagelin, D. V. Nanopoulos, K. A. Olive, and M. Srednicki, Supersymmetric Relics from the Big Bang, Nucl. Phys. B **238**, 453 (1984).

[6] J. L. Feng and J. Kumar, The WIMPless Miracle: Dark-Matter Particles without Weak-Scale Masses or Weak Interactions, Phys. Rev. Lett. **101**, 231301 (2008), arXiv:0803.4196 [hep-ph].

[7] P. Gondolo and G. Gelmini, Cosmic abundances of stable particles: Improved analysis, Nucl. Phys. B **360**, 145 (1991).

[8] J. Edsjö and P. Gondolo, Neutralino relic density including coannihilations, Phys. Rev. D **56**, 1879 (1997), arXiv:hep-ph/9704361.

[9] M. Ackermann *et al.* (Fermi-LAT), Searching for Dark Matter Annihilation from Milky Way Dwarf Spheroidal Galaxies with Six Years of Fermi Large Area Telescope Data, Phys. Rev. Lett. **115**, 231301 (2015), arXiv:1503.02641 [astro-ph.HE].

[10] V. Acciari *et al.* (MAGIC), A search for dark matter in Triangulum II with the MAGIC telescopes, Phys. Dark Univ. **28**, 100529 (2020), arXiv:2003.05260 [astro-ph.HE].

[11] M. Ahnen *et al.* (MAGIC), Indirect dark matter searches in the dwarf satellite galaxy Ursa Major II with the MAGIC Telescopes, JCAP **03**, 009, arXiv:1712.03095 [astro-ph.HE].

[12] A. Morselli (CTA Consortium), The Dark Matter Programme of the Cherenkov Telescope Array, PoS **ICRC2017**, 921 (2018), arXiv:1709.01483 [astro-ph.IM].

[13] R. Mukherjee (VERITAS), Observing the Energetic Universe at Very High Energies with the VERITAS Gamma Ray Observatory, Adv. Space Res. **62**, 2828 (2018), arXiv:1809.10285 [astro-ph.HE].

[14] T. Bringmann, J. Edsjö, P. Gondolo, P. Ullio, and L. Bergström, DarkSUSY 6 : An Advanced Tool to Compute Dark Matter Properties Numerically, JCAP **07**, 033, arXiv:1802.03399 [hep-ph].

[15] F. Ambrogi, C. Arina, M. Backovic, J. Heisig, F. Maltoni, L. Mantani, O. Mattelaer, and G. Mohlabeng, MadDM v.3.0: a Comprehensive Tool for Dark Matter Studies, Phys. Dark Univ. **24**, 100249 (2019), arXiv:1804.00044 [hep-ph].

[16] G. Belanger, F. Boudjema, A. Pukhov, and A. Semenov, MicrOMEGAs 2.0: A Program to calculate the relic density of dark matter in a generic model, Comput. Phys. Commun. **176**, 367 (2007), arXiv:hep-ph/0607059.

[17] A. Arbey and F. Mahmoudi, SuperIso Relic: A Program for calculating relic density and flavor physics observables in Supersymmetry, Comput. Phys. Commun. **181**, 1277 (2010), arXiv:0906.0369 [hep-ph].

[18] M. Pospelov, A. Ritz, and M. B. Voloshin, Secluded WIMP Dark Matter, Phys. Lett. B **662**, 53 (2008), arXiv:0711.4866 [hep-ph].

[19] J. L. Feng, H. Tu, and H.-B. Yu, Thermal Relics in Hidden Sectors, JCAP **10**, 043, arXiv:0808.2318 [hep-ph].

[20] M. Pospelov, Secluded U(1) below the weak scale, Phys. Rev. D **80**, 095002 (2009), arXiv:0811.1030 [hep-ph].

[21] K. Sigurdson, Hidden Hot Dark Matter as Cold Dark Matter, (2009), arXiv:0912.2346 [astro-ph.CO].

[22] C. Cheung, G. Elor, L. J. Hall, and P. Kumar, Origins of Hidden Sector Dark Matter I: Cosmology, JHEP **03**, 042, arXiv:1010.0022 [hep-ph].

[23] G. Arcadi, M. Dutra, P. Ghosh, M. Lindner, Y. Mambrini, M. Pierre, S. Profumo, and F. S. Queiroz, The waning of the WIMP? A review of models, searches, and constraints, Eur. Phys. J. C **78**, 203 (2018), arXiv:1703.07364 [hep-ph].

[24] G. Bertone and M. Tait, Tim, A new era in the search for dark matter, Nature **562**, 51 (2018), arXiv:1810.01668 [astro-ph.CO].

[25] J. Beacham *et al.*, Physics Beyond Colliders at CERN: Beyond the Standard Model Working Group Report, J. Phys. G **47**, 010501 (2020), arXiv:1901.09966 [hep-ex].

[26] M. Pospelov and A. Ritz, Astrophysical Signatures of Secluded Dark Matter, Phys. Lett. **B671**, 391 (2009), arXiv:0810.1502 [hep-ph].

[27] J. Mardon, Y. Nomura, D. Stolarski, and J. Thaler, Dark Matter Signals from Cascade Annihilations, JCAP **05**, 016, arXiv:0901.2926 [hep-ph].

[28] K. Schmidt-Hoberg, F. Staub, and M. W. Winkler, Constraints on light mediators: confronting dark matter searches with B physics, Phys. Lett. B **727**, 506 (2013), arXiv:1310.6752 [hep-ph].

[29] S. Tulin, H.-B. Yu, and K. M. Zurek, Beyond Collisionless Dark Matter: Particle Physics Dynamics for Dark Matter Halo Structure, Phys. Rev. D **87**, 115007 (2013), arXiv:1302.3898 [hep-ph].

[30] S. Alekhin *et al.*, A facility to Search for Hidden Particles at the CERN SPS: the SHiP physics case, Rept. Prog. Phys. **79**, 124201 (2016), arXiv:1504.04855 [hep-ph].

[31] M. Hufnagel, K. Schmidt-Hoberg, and S. Wild, BBN constraints on MeV-scale dark sectors. Part I. Sterile decays, JCAP **02**, 044, arXiv:1712.03972 [hep-ph].

[32] F. Kahlhoefer, K. Schmidt-Hoberg, and S. Wild, Dark matter self-interactions from a general spin-0 mediator, JCAP **08**, 003, arXiv:1704.02149 [hep-ph].

[33] K. Bondarenko, A. Boyarsky, T. Bringmann, M. Hufnagel, K. Schmidt-Hoberg, and A. Sokolenko, Direct detection and complementary constraints for sub-GeV dark matter, JHEP **03**, 118, arXiv:1909.08632 [hep-ph].

[34] R. T. D'Agnolo and J. T. Ruderman, Light Dark Matter from Forbidden Channels, Phys. Rev. Lett. **115**, 061301 (2015), arXiv:1505.07107 [hep-ph].

[35] D. Pappadopulo, J. T. Ruderman, and G. Trevisan, Dark matter freeze-out in a nonrelativistic sector, Phys. Rev. D **94**, 035005 (2016), arXiv:1602.04219 [hep-ph].

[36] A. Berlin, D. Hooper, and G. Krnjaic, Thermal Dark Matter From A Highly Decoupled Sector, Phys. Rev. D **94**, 095019 (2016), arXiv:1609.02555 [hep-ph].

[37] G. Steigman, B. Dasgupta, and J. F. Beacom, Precise Relic WIMP Abundance and its Impact on Searches for Dark Matter Annihilation, Phys. Rev. **D86**, 023506 (2012), arXiv:1204.3622 [hep-ph].

[38] T. Bringmann, Particle Models and the Small-Scale Structure of Dark Matter, New J. Phys. **11**, 105027 (2009), arXiv:0903.0189 [astro-ph.CO].

[39] T. Binder, T. Bringmann, M. Gustafsson, and A. Hryczuk, Early kinetic decoupling of dark matter: when the standard way of calculating the thermal relic density fails, Phys. Rev. D **96**, 115010 (2017), arXiv:1706.07433 [astro-ph.CO].

[40] M. Drees, F. Hajkarim, and E. R. Schmitz, The Effects of QCD Equation of State on the Relic Density of WIMP Dark Matter, JCAP **1506** (06), 025, arXiv:1503.03513 [hep-ph].

[41] N. Arkani-Hamed, D. P. Finkbeiner, T. R. Slatyer, and N. Weiner, A Theory of Dark Matter, Phys. Rev. D **79**, 015014 (2009), arXiv:0810.0713 [hep-ph].

[42] L. Ackerman, M. R. Buckley, S. M. Carroll, and M. Kamionkowski, Dark Matter and Dark Radiation, , 277 (2008), arXiv:0810.5126 [hep-ph].

[43] B. Batell, M. Pospelov, and A. Ritz, Probing a Secluded U(1) at B-factories, Phys. Rev. D **79**, 115008 (2009), arXiv:0903.0363 [hep-ph].

[44] J. Alexander *et al.*, Dark Sectors 2016 Workshop: Community Report (2016) arXiv:1608.08632 [hep-ph].

[45] T. Bringmann, F. Kahlhoefer, K. Schmidt-Hoberg, and P. Walia, Strong constraints on self-interacting dark matter with light mediators, Phys. Rev. Lett. **118**, 141802 (2017), arXiv:1612.00845 [hep-ph].

[46] T. Bringmann, F. Kahlhoefer, K. Schmidt-Hoberg, and P. Walia, Converting nonrelativistic dark matter to radiation, Phys. Rev. D **98**, 023543 (2018), arXiv:1803.03644 [astro-ph.CO].

[47] J. L. Feng, M. Kaplinghat, H. Tu, and H.-B. Yu, Hidden Charged Dark Matter, JCAP **07**, 004, arXiv:0905.3039

[hep-ph].

[48] L. G. van den Aarssen, T. Bringmann, and C. Pfrommer, Is dark matter with long-range interactions a solution to all small-scale problems of ΛCDM cosmology?, Phys. Rev. Lett. **109**, 231301 (2012), arXiv:1205.5809 [astro-ph.CO].

[49] M. Kaplinghat, S. Tulin, and H.-B. Yu, Direct Detection Portals for Self-interacting Dark Matter, Phys. Rev. D **89**, 035009 (2014), arXiv:1310.7945 [hep-ph].

[50] M. Cirelli, P. Panci, K. Petraki, F. Sala, and M. Taoso, Dark Matter's secret liaisons: phenomenology of a dark U(1) sector with bound states, JCAP **05**, 036, arXiv:1612.07295 [hep-ph].

[51] P. Ade *et al.* (Simons Observatory), The Simons Observatory: Science goals and forecasts, JCAP **02**, 056, arXiv:1808.07445 [astro-ph.CO].

[52] K. Abazajian *et al.*, CMB-S4 Science Case, Reference Design, and Project Plan, (2019), arXiv:1907.04473 [astro-ph.IM].

[53] A. Berlin, D. Hooper, and G. Krnjaic, PeV-Scale Dark Matter as a Thermal Relic of a Decoupled Sector, Phys. Lett. B **760**, 106 (2016), arXiv:1602.08490 [hep-ph].

[54] M. Cirelli, Y. Gouttenoire, K. Petraki, and F. Sala, Homeopathic Dark Matter, or how diluted heavy substances produce high energy cosmic rays, JCAP **02**, 014, arXiv:1811.03608 [hep-ph].

[55] M. Hufnagel, K. Schmidt-Hoberg, and S. Wild, BBN constraints on MeV-scale dark sectors. Part II. Electromagnetic decays, JCAP **11**, 032, arXiv:1808.09324 [hep-ph].

[56] M. J. Dolan, F. Kahlhoefer, C. McCabe, and K. Schmidt-Hoberg, A taste of dark matter: Flavour constraints on pseudoscalar mediators, JHEP **03**, 171, [Erratum: JHEP 07, 103 (2015)], arXiv:1412.5174 [hep-ph].

[57] J. A. Evans, S. Gori, and J. Shelton, Looking for the WIMP Next Door, JHEP **02**, 100, arXiv:1712.03974 [hep-ph].

[58] M. W. Winkler, Decay and detection of a light scalar boson mixing with the Higgs boson, Phys. Rev. D **99**, 015018 (2019), arXiv:1809.01876 [hep-ph].

[59] G. Elor, N. L. Rodd, T. R. Slatyer, and W. Xue, Model-Independent Indirect Detection Constraints on Hidden Sector Dark Matter, JCAP **06**, 024, arXiv:1511.08787 [hep-ph].

[60] E. D. Carlson, M. E. Machacek, and L. J. Hall, Self-interacting dark matter, Astrophys. J. **398**, 43 (1992).

[61] Y. Hochberg, E. Kuflik, T. Volansky, and J. G. Wacker, Mechanism for Thermal Relic Dark Matter of Strongly Interacting Massive Particles, Phys. Rev. Lett. **113**, 171301 (2014), arXiv:1402.5143 [hep-ph].

[62] N. Bernal, X. Chu, C. Garcia-Cely, T. Hambye, and B. Zaldivar, Production Regimes for Self-Interacting Dark Matter, JCAP **03**, 018, arXiv:1510.08063 [hep-ph].

[63] D. E. Kaplan, M. A. Luty, and K. M. Zurek, Asymmetric Dark Matter, Phys. Rev. D **79**, 115016 (2009), arXiv:0901.4117 [hep-ph].

[64] L. J. Hall, K. Jedamzik, J. March-Russell, and S. M. West, Freeze-In Production of FIMP Dark Matter, JHEP **03**, 080, arXiv:0911.1120 [hep-ph].

[65] L. J. Hall, J. March-Russell, and S. M. West, A Unified Theory of Matter Genesis: Asymmetric Freeze-In, (2010), arXiv:1010.0245 [hep-ph].

[66] R. J. Scherrer and M. S. Turner, On the Relic, Cosmic Abundance of Stable Weakly Interacting Massive Particles, Phys. Rev. D **33**, 1585 (1986), [Erratum: Phys.Rev.D 34, 3263 (1986)].